

Date of publication xxxx 00, 0000, date of current version xxxx 00, 0000.

Digital Object Identifier 10.1109/ACCESS.2025.DOI

Design and Comparative Analysis of Electric Motors with "Flux-Switching" Effect Having Reluctance Rotors and PM or DC Stator Excitation

OLUWASEUN A. BADEWA¹, (Graduate Student Member, IEEE), ALI MOHAMMADI², (Senior Member, IEEE), DONOVIN D. LEWIS¹, (Member, IEEE), SOMASUNDARAM ESSAKIAPPAN³, (Senior Member, IEEE), MADHAV D. MANJREKAR³, (Senior Member, IEEE), and DAN M. IONEL¹, (Fellow, IEEE)

¹SPARK Laboratory, Stanley and Karen Pigman College of Engineering, University of Kentucky, Lexington, KY, USA (e-mail: o.badewa@uky.edu, donovin.lewis@uky.edu, and dan.ionel@ieee.org)

²Nidec Motor Corporation, St. Louis, Missouri, USA (e-mail: ali.mohammadi@ieee.org)

Corresponding author: Oluwaseun A. Badewa (e-mail: o.badewa@uky.edu).

ABSTRACT This paper introduces innovative designs for synchronous electric motors with phase coils and permanent magnets (PM) or DC-excitation coils embedded in the stator. Alongside concentrated phase coils in dedicated slots, the spoke-type PMs offer high flux intensification, while the option for DCexcitation coils eliminates demagnetization risks. Since the rotor has no active electromagnetic components, the machine can achieve high-speed operation while enabling advanced cooling systems focused solely on the stator. A special implementation with a "wave" or "serpentine" DC-excitation winding which has the potential for reduced losses depending on the motor aspect ratio is presented. The operation, control, and polarity of the DC-excited variant are analyzed using analytical equations and an examination of the airgap field. The design of experiment-based sensitivity analyses and multi-objective optimization employing differential evolution (MODE) is used to analyze the machine topologies for a power rating of 100kW motor at a speed of 3,000rpm, which is typical for industrial applications. The conflicting objectives of maximizing average torque and minimizing motor losses are considered in both the inner and outer rotor configurations of the proposed motor topologies. Discussions on the performance of the selected "best" designs from each topology and their competitiveness compared to state-of-the-art motors are presented. A DC-excited outer rotor design is analyzed and proposed for EV applications, considering different drive cycles, and a prototype of a PM inner rotor design is constructed and tested, showing competitive performance even at high operating temperatures.

INDEX TERMS Electric machine, synchronous motor, flux-intensifying topology, flux switching, flux modulation, variable flux, spoke permanent magnet, DC excitation, FEA.

I. INTRODUCTION

Continuous improvement in the performance of electrical machines is a prerequisite for keeping up with the ever-changing sustainability needs of this global electrification era [1]. Computer-aided simulations such as finite element analysis (FEA) and analytical methods are typical tools used for designing and optimizing electrical machines to meet these needs [2]. The results obtained from these computational approaches enable comparative performance assessments,

facilitating the selection of optimal motor topologies tailored to the specific demands of diverse applications, given the large array of available choices.

The current paper investigates and comparatively analyses special motor topologies with stator-only excitation employing either permanent magnets (PMs) or DC-excitation windings placed in the stator and AC armature windings working with a reluctance rotor. These machines belong to the general class of hybrid excited synchronous machines,

³University of North Carolina at Charlotte, Charlotte, NC, USA (e-mail: soma.e@ieee.org, madhav.manjrekar@uncc.edu)

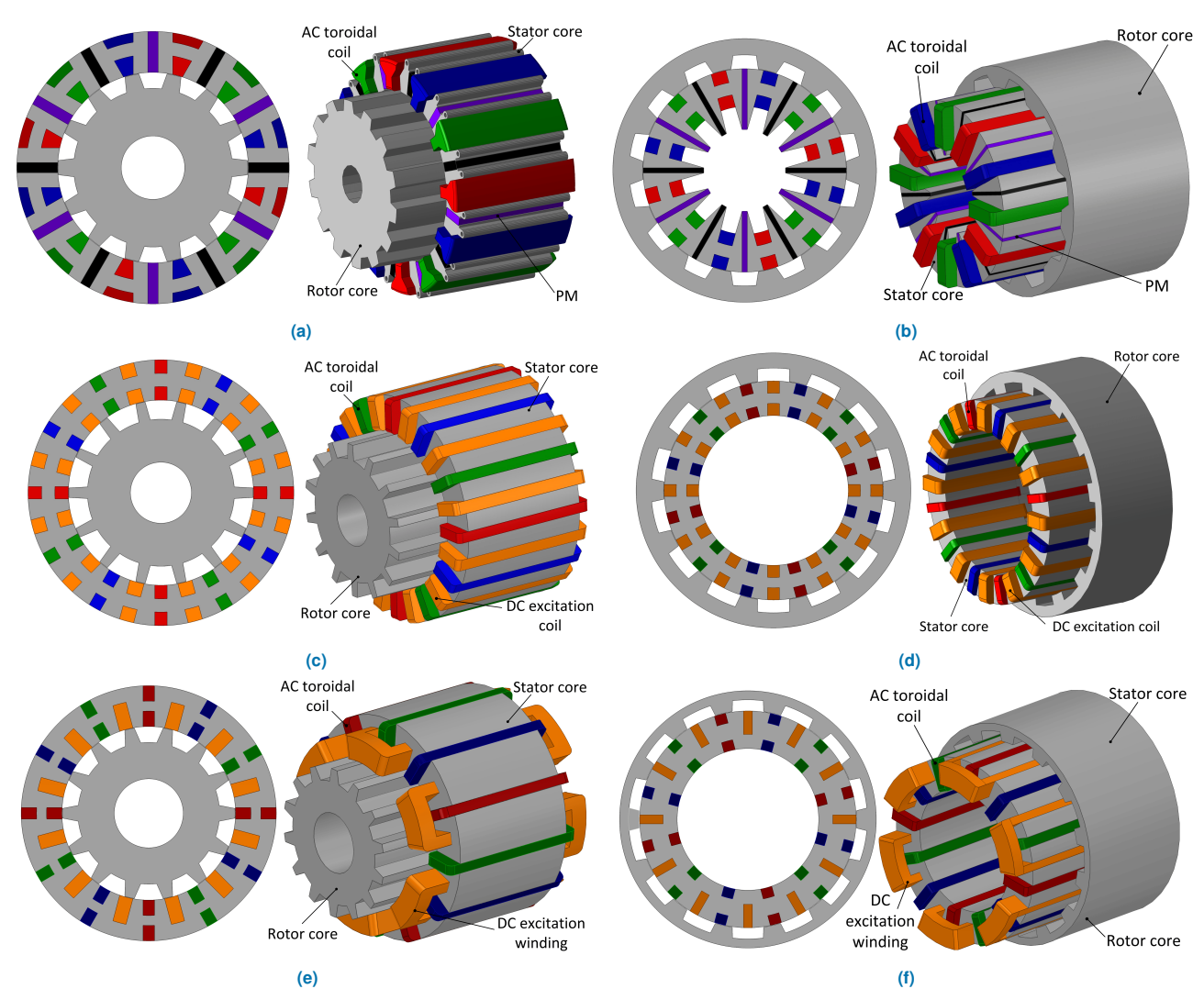


FIGURE 1. Exploded and cross-sectional views of motor topologies with (a) inner rotor PM-excitation (IR-PM), (b) outer rotor PM-excitation (OR-PM), (c) inner rotor DC-excitation (IR-DC), (d) outer rotor DC-excitation (OR-DC), (e) inner rotor wave DC-excitation (IR-WDC), and (f) outer rotor wave DC-excitation (OR-WDC).

operating with a rotating fundamental field as documented in [3]–[7]. They employ a repetitive structure of circumferentially placed modules in the stator, each comprising either DC-excitation coils or PMs that are arranged radially and magnetized tangentially. Each stator module also includes a single concentrated toroidal coil, wound around the core, and belonging to one of the three-phase AC windings. The rotors feature alternating protrusions that create a single flux barrier effect and contain no active elements, allowing for high-speed operations [7]. A novel implementation of a DC-excitation winding is presented, potentially providing a tradeoff in performance between the PM and DC-excited toroidal AC winding machines.

The earliest implementations of these machine topologies go as far back as the 1920s with the "induction-type" synchronous motor documented by Carr et al. [8] and in the 1950s, an alternator with a dual set of windings in the stator and a reluctance rotor investigated by Gupta et al. [9] as well as a "flux-switching" alternator developed by Rauch

and Johnson [10]. Several variants have been documented, including those referred to as "doubly salient" PM [11], "flux reversal" doubly salient [12], "PM synchronous" [13], "synchronous rotor DC-excited" [14], amongst others. The class referred to as "flux reversal" or "flux switching" machines (FSM) claims enhanced efficiency and high power density, with reduced or zero reliance on rare-earth materials, making them an attractive option for industrial applications [15], [16].

These "flux-switching," "flux-reversal," or "variable-flux" machines are nothing but synchronous machines whose excitation is a result of the combined effect of the PM or DC excitation and the rotor reluctance [7], [17]. Their operation is based on the principle of variable flux linkage, such that the induced EMF interacts with an alternating armature current. While the field excitation is provided by magnets or DC coils, the flux linkage of the armature windings changes by the variation of the magnetic circuit reluctance as the rotor rotates, such that an alternating EMF is induced without

rotating PMs or excitation coils [12], [18].

An extensive review of PM excited versions of "fluxswitching" machines was carried out by Chen et al. [16], highlighting, for example, how outer-rotor configurations with V-shaped or wedge-shaped magnets improve "torque density" and "flux-weakening capability" compared to conventional designs. Goli et al. [19] also proposed that a special implementation of this motor topology can meet the 50kW/L "power density target" set by the department of energy (DOE) through modular stator windings and reluctance rotors, achieving fault tolerance and high-speed operation while maintaining sinusoidal back-EMF characteristics. Badewa et al. [7] investigated inner and outer rotor designs for "high power density applications" and possible use of ferrites, demonstrating that spoke-type PM arrangements enable optimal magnet utilization through flux intensification and that cost-effective non-rare earth PMs can be employed without sacrificing performance.

Further approaches to improve the performance of the PM versions have been proposed in the literature. For example, Faiz et al. [20] proposed this PM topology for "EV traction applications", recommending hybrid magnet systems (Nd+Al-Ni-Co) to balance torque density and flux weakening, though noting limitations in reluctance torque compared to IPMSMs. Idoko et al. [21] suggested that using a "dual stator" configuration further benefits this topology, showing 43.5% higher specific torque and 75.9% lower torque ripple in optimized designs. Schneider et al. [22] proposed "nanocomposite materials" as a means of improvement, achieving rare-earth-free axial FSPM machines with 6.1 kW/kg power density through metal amorphous cores, though requiring advanced manufacturing for high-frequency operation.

On the other hand, investigations have been made into DC-excited or hybrid excitation variations, as a means to reduce the reliance on rare-earth PMs, avoid demagnetization concerns, amongst other proposed benefits. Badewa et al. [23] demonstrated that "DC-excited stator synchronous machines" offer competitive performance for propulsion, achieving higher "specific power" especially at larger diameters and fault-tolerant operation while eliminating PM demagnetization risks. Boldea et al. [18] analyzed "DC flux-switching machines" as switched reluctance motor (SRM) alternatives, noting their compatibility with PWM inverters but highlighting challenges like high current density and lower power factor as compared to their PM counterparts.

Ullah et al. [24] developed a "modular E-shaped stator" hybrid excited motor that combines PMs and DC field windings, achieving 62% higher "torque density" through genetic optimization while reducing PM volume by 36%. Their design's "flux gaps" enabled simultaneous flux regulation and 21% lower torque ripple, demonstrating how DC excitation complements PMs in high-performance applications. Ali et al. [25]'s review of "double stator machines" confirmed that parallel hybrid excitation topologies outperform pure DC-excited versions in torque density, but noted DC variants

remain valuable for avoiding PM demagnetization risks in harsh environments.

This paper expands on the authors' group extensive research on the concept machine topologies, which are being studied in DOE VTO and NASA-funded projects for high power density applications in multi-MW direct drive generators by Mohammadi et al. [26], EV traction motors by Badewa et al. [27], [28], and more recently, electric propulsion [29], [30]. Each section brings substantial new contributions, as briefly described in the following. In the next section, possible arrangements with inner and outer stators, and with PM and DC excitation, are introduced. The operational analysis of the motor topology is detailed, considering the synchronous excitation provided by the stator components and their field interactions with a reluctance rotor of suitable polarity in Section III. The comparative systematic optimal design-of-study from Section IV includes a design of experiment-based sensitivity analyses for the various motor topologies and a multi-objective differential evolution-based optimization. Optimal designs of the different topologies are comparatively analyzed for typical performance indexes to identify their relative merits. An example selected design is analyzed for EV application, considering various drive cycles, together with prototyping, testing, and successful experimental validation in Section V, which is followed by a conclusion.

II. MOTOR TOPOLOGIES

The proposed novel machine topologies have implementations in inner and outer rotor configurations with PM or DC excitation in the stator as shown in Figs 1a - d, with a special DC excitation "wave" winding configuration shown in Figs 1e - f [31]. The stator in the inner rotor (IR-) or outer rotor (OR-) PM-excited variants can be made into multiple modules, each with a PM and single concentration coil part of a phase winding while in the DC-excited variants, a stator module would contain two toroidal coils belonging to one AC phase and a DC-excitation winding or a special implementation with a "wave" or "serpentine" DC-excitation winding which has the potential for reduced losses depending on the motor aspect ratio.

This modular stator design features rectangular slots that accommodate rectangular wire, resulting in a high slot fill factor and minimal copper losses. The concentrated coils are toroidally wound with compact axial ends, further reducing copper losses. The winding arrangement follows the sequence of the three phases around the stator's circumference, with high fault tolerance achieved by placing only one coil side in each slot. Permanent magnets (PMs) are also arranged radially in the stator, with every two consecutive magnets tangentially magnetized in opposite directions. The DC-excited variants see these PMs replaced with excitation windings with the same purpose.

The rotor has no active excitation components and consists of a laminated steel core of reluctance type with protrusions. The number and size of these protrusions will be shown to

match the stator's characteristics. This simple rotor design enables high-speed operation, contributing to extended range and high power density.

The high cost of rare-earth permanent magnets (PMs) has long been a concern in PM-excited machines. The outer rotor configuration offers an option for reducing costs by using longer, lower-cost PMs, such as non-rare-earth types like iron nitride or ferrites, in larger quantities within the same volume. This can achieve comparable performance to rare-earth PM designs while lowering the overall cost [32], [33]. The concerns of cost and demagnetization associated with PMs are eliminated in the DC-excited variants, allowing for high electrical loading, provided sufficient cooling is available.

The subsequent sections will provide a more detailed analysis of the motor topologies, their operation, and potential benefits. It is worth noting that these motor topologies face some challenges, including eddy currents and other losses due to strong magnetic field variations caused by open slots, along with high common-mode current and electromagnetic interference (EMI) issues linked to toroidal windings [34]–[36]. These challenges can be mitigated through design optimizations such as smaller slot openings, using Litz wire, and other advanced techniques [37].

III. OPERATIONAL ANALYSIS

In previous works, the concept of flux intensification through the arrangement of toroidal windings as well as PM placements has been validated through electromagnetic simulations as well as from prototypes [2], [17]. The operation of the PM-excited machine has also been explained through mmf analysis and airgap field analysis as detailed in [17].

A similar approach will be applied in this section to complement the existing work by investigating the operation of the DC-excited variants, whose operation is similar in that the PMs are replaced as the source of excitation with DC coils [28]. The DC coil sides are optimally placed in the stator core and can be supplied in the simplest implementation with an uncontrolled DC voltage source to produce the excitation field.

The electromagnetic performance of this machine is based on the interaction of the excitation flux produced by the DC-excitation windings, ϕ_{ex} , the flux due to the armature magnetic reaction, ϕ_{arm} , and the rotor. The armature flux linkage between the active stator and castellated rotor, ϕ_{AM} , can therefore be defined as the vector sum given by:

$$\vec{\phi_{AM}} = \vec{\phi_{ex}} + \vec{\phi_{arm}},\tag{1}$$

This interaction provides the advantage of several degrees of freedom in this machine as regards motor control in the constant power and flux weakening regions. The armature voltage, V, can then be expressed as:

$$V = \phi_{AM} \cdot \omega \cdot p, \tag{2}$$

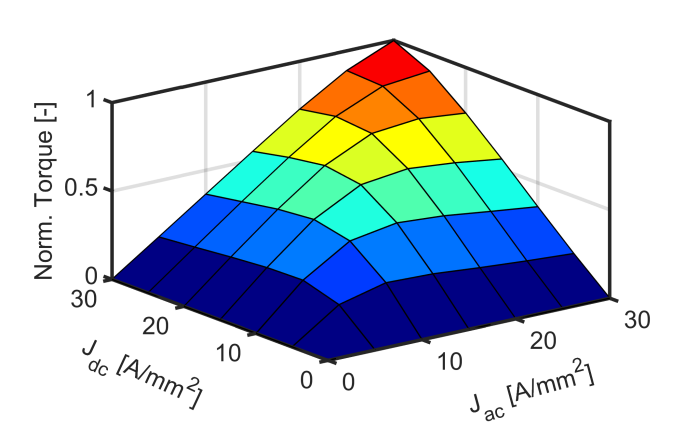


FIGURE 2. Example control characteristics for proposed motor design through AC supply, and DC excitation control.

where ω is the mechanical speed, and p is the number of pole pairs. The voltage drop across the resistance of the winding is assumed to be minimal, and the less dominant element, especially at high operating speeds.

The electromagnetic torque, T_{emq} , can also be derived as:

$$T_{emg} = p \cdot \phi_{ex} \cdot I \cdot \cos(\theta),$$

= $p \cdot (\phi_{ex} \cdot i_q + (L_d - L_q) \cdot i_d \cdot i_q),$ (3)

where I is the armature current, L_{dq} , and i_{dq} are the components of motor inductance and current in the d- and q-axes, respectively. As such a generalized expression of the total armature flux can be gotten as:

$$\phi_{AM} = \sqrt{(\phi_{exc} - L \cdot I \cdot \sin(\theta))^2 + (L \cdot I \cdot \cos(\theta))^2}, (4)$$

This relationship provides several options for control, especially in the constant power region where flux weakening can be achieved through one or a combination of:

- 1) Adjusting the modulus of the armature current, I,
- 2) Adjusting the phase shift of the current with respect to the EMF, θ , or
- 3) Excitation flux control, $\vec{\phi}_{ex}$.

Therefore, at any given speed, the desired torque can be achieved by varying the combinations of AC current density, J_{ac} , and DC excitation current density, J_{dc} , as depicted in Fig. 2. A direct consequence of the freedom of control is the ability of this machine to operate with an effective power factor, allowing for a better dimensioning of the converter-machine assembly.

For optimal performance, the active stator in the machine is electromagnetically coordinated with the rotor such that an investigation of the airgap field produced by the excitation coils and their interaction with the armature windings can provide insight into the feasible polarities of this machine. Considering an example 24-slot OR-DC machine as shown in Fig. 1d, the The concept of a half airgap is used to study the influence of the active stator and rotor on the airgap flux.

The airgap flux produced by a stator with only DC-excitation coils is studied. Initially, the rotor is assumed to have a smooth surface with no protrusions. The harmonic spectrum of the airgap flux, B_g , is presented in Fig. 3. The harmonic analysis shows that the principal harmonics present are in odd multiples of the pole pair number of the DC-excitation coils, in this case, 6.

A castellated rotor is then introduced to the stator with only DC-excitation coils constituting an open-circuit condition for this example machine. The rotor has an example number of protrusions, N_{pr} , equal 14, and B_g is analyzed as in Fig. 3b. The previously dominant harmonics due to the DC-excitation coils are suppressed, and the dominant harmonic equals N_{pr} .

A full load condition is then analyzed with the addition of energized 3-phase AC coils, along with the DC-excitation coils, and the castellated rotor. The analyzed B_g in Fig. 4 shows that the prominent harmonics are a combination in between the number of rotor protrusions, N_{pr} , and the number of the DC-excitation coils. The dominant harmonic, which determines the polarity of the machine, in this example machine, is 14, which corresponds to N_{pr} . Other smaller harmonics, which are multiples of dominant harmonics and resultant of the interaction between stator and rotor, can be further reduced through skewing and advanced rotor tooth shaping [38]. Therefore, in line with expectations with either DC or PM-excitation, the polarity of this machine topology is determined by the number of rotor protrusions, N_{pr} .

IV. COMPARATIVE OPTIMIZATION STUDIES

Comparative analysis of the proposed designs is carried out using a mixture of design of experiments, sensitivity analysis, and multi-objective differential evolution optimization. Considerations for manufacturing, prototyping, and applications of these electric machines are also discussed, considering typical critical factors.

A. DESIGN OF EXPERIMENTS (DOE)-BASED SENSITIVITY ANALYSIS

Experimentally validated 2D parametric models of the inner rotor DC-excited (IR-DC), outer rotor DC-excited (OR-DC), inner rotor PM-excited (IR-PM), and outer rotor PM-excited (OR-PM) motor topologies were developed for comparative analysis, as shown in Figs. 5 and 6. It is assumed that the special design with the DC wave winding would have similar characteristics to the DC toroidal winding designs in most aspects. Each design had 8 - 11 independent geometrical variables as described in Tables 1 - 4. The stator and rotor pole pitches are represented by τ_s and τ_r , respectively. These geometrical variables are dimensionless ratios related to lengths and pole pitches in the stator and rotor. An airgap, g, of 0.5mm, and a slot fill factor (SFF) of 0.5, which is typically feasible with hand-wound coils, are considered in all models, along with a high-performance AK-steel HF-10 in the stator and rotor. Also, a minimum magnet thickness of 1mm was considered in the models, which is well within manufacturing tolerances [39], [40]. These developed models

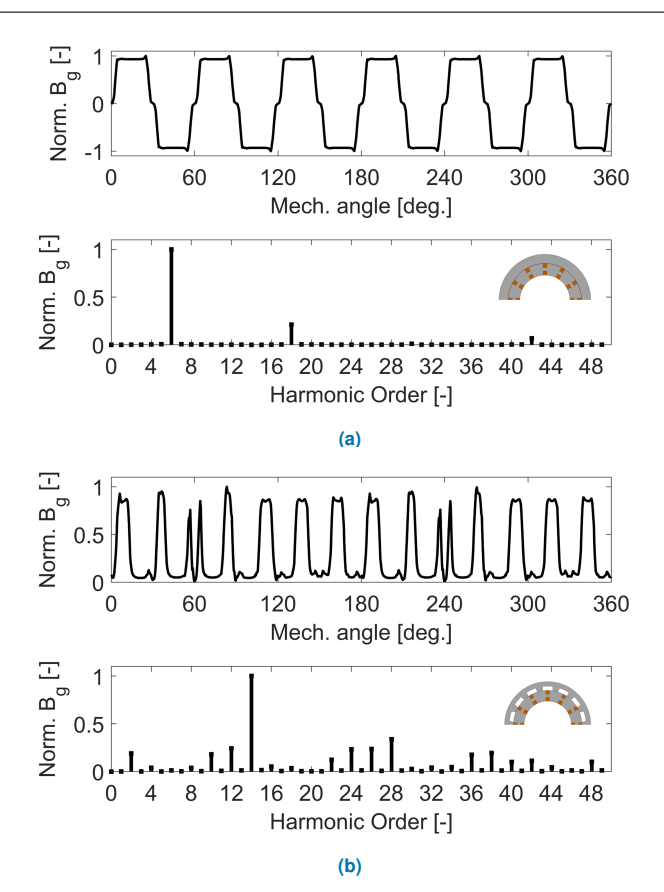


FIGURE 3. Open circuit airgap flux and harmonic decomposition for computational models with (a) only DC-excitation coils in the stator and a smooth rotor showing harmonics in multiples of the slot number, (b) only DC-excitation coils in the stator with a castellated rotor, indicating a strong 14th harmonic corresponding to the number of rotor protrusions.

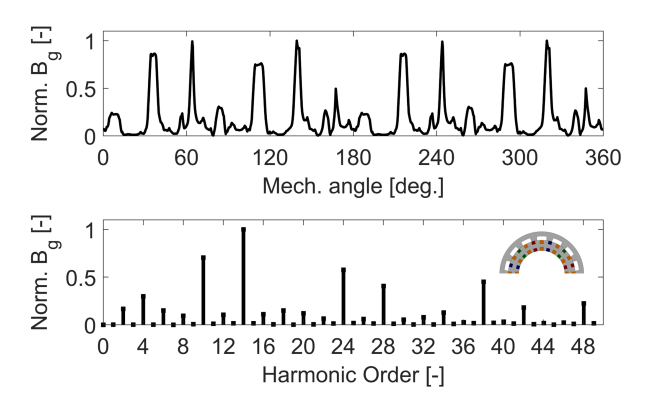


FIGURE 4. Modulus of the airgap flux density calculated based on the radial and tangential components for the computational model with DC-excitation coils, toroidal AC coils, stator, and castellated rotor, illustrating that the largest harmonic component is the 14th.

leverage extensive optimization findings and experimental data obtained using a small-scale open-frame lab prototype developed as part of a larger DOE VTO and NASA ULI project. This provided a prior opportunity for experimental validation, including that for torque, loss, and mechanical stability, as documented in [7], [19], [41].

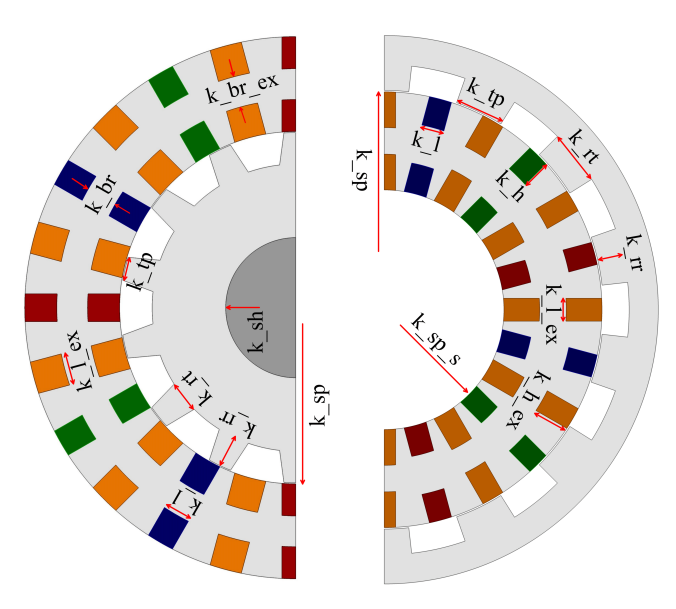


FIGURE 5. Cross-sectional view of IR-DC and OR-DC designs with labeled geometric independent variables considered in the sensitivity analysis and multi-objective optimization.

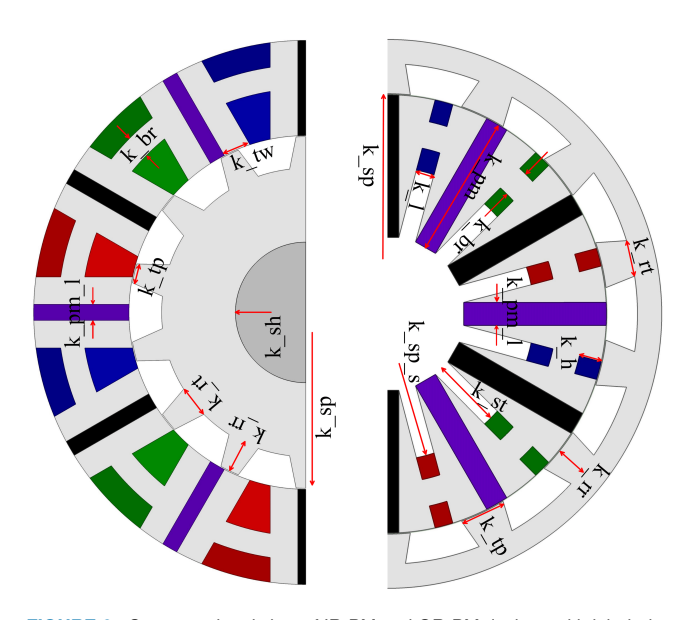


FIGURE 6. Cross-sectional view of IR-PM and OR-PM designs with labeled geometric independent variables considered in the sensitivity analysis and multi-objective optimization.

Sensitivity analyses were utilized to examine the impact of varying geometric variables on the machine topology performances relating to torque output, T_e , torque ripple, T_r , motor loss, W_t , and power factor, pf, at peak loading of 30A/mm^2 [42], [43]. The 2D parametric models used have been experimentally verified to provide satisfactory accuracy in computing performance values, and for one order of magnitude less time than 3D models. This makes them computationally efficient for large-scale design optimization and comparative analyses. Additionally, an optimal mesh analysis was performed to ensure satisfactory results within a reasonable solve time. Critical regions such as the stator

TABLE 1. Independent variables for the IR-DC design optimization, and their ranges.

Variable	Description	Min	Max
k_sp	split ratio = $\frac{ID_s}{OD_s}$	0.60	0.70
k_l	ac slot width ratio = $\frac{\omega_{slot_ac}}{\tau_s}$	0.25	0.35
k_br	ac bridge length ratio = $\frac{2 \cdot \ell_{bridge_ac}}{OD_s - ID_s}$	0.30	0.35
k_l_ex	dc slot width ratio = $\frac{\omega_{slot_dc}}{\tau_s}$	0.30	0.35
k_br_ex	dc bridge length ratio = $\frac{2 \cdot \ell_{bridge_dc}}{OD_s - ID_s}$	0.30	0.35
k_sh	shaft dia. ratio = $\frac{OD_{shaft}}{OD_r}$	0.30	0.50
k_tp	rotor pole top ratio = $\frac{\tau_{r_top}}{\tau_r}$	0.40	0.80
k_rt	rotor pole root ratio = $\frac{\tau_{r_rroot}}{\tau_r}$	0.35	0.65
k_rr	rotor pole depth ratio = $\frac{\ell_{rpd}}{OD_r - ID_r}$	0.20	0.40

TABLE 2. Independent variables for the OR-DC design optimization, and their ranges.

Variable	Description	Min	Max
k_sp	split ratio = $\frac{ID_r}{OD_r}$	0.75	0.80
k_sp_s	stator split ratio = $\frac{ID_s}{OD_s}$	0.55	0.70
k_h	ac slot length ratio = $\frac{2 \cdot \ell_{slot} ac}{OD_s - ID_s}$	0.30	0.35
k_l	ac slot width ratio = $\frac{\omega_{slot_ac}}{\tau_s}$	0.20	0.23
k_h_ex	dc slot length ratio = $\frac{2 \cdot \ell_{slot_dc}}{OD_s - ID_s}$	0.30	0.35
k_l_ex	dc slot width ratio = $\frac{\omega_{slot_dc}}{\tau_s}$	0.20	0.23
k_tp	rotor pole top ratio = $\frac{\tau_{r_top}}{\tau_r}$	0.30	0.50
k_rt	rotor pole root ratio = $\frac{\tau_{r_root}}{\tau_r}$	0.40	0.70
k_rr	rotor pole depth ratio = $\frac{\ell_{rpd}}{OD_r - ID_r}$	0.40	0.50

TABLE 3. Independent variables for the IR-PM design optimization, and their ranges.

Variable	Description	Min	Max
k_sp	split ratio = $\frac{ID_s}{OD_s}$	0.60	0.70
k_pm_l	PM width ratio = $\frac{\omega_{PM}}{g}$	10.00	20.00
k_br	bridge length ratio = $\frac{2 \cdot \ell_{bridge}}{OD_s - ID_s}$	0.17	0.33
k_tw	stator tooth width ratio = $\frac{\omega_{tooth}}{\tau_s}$	0.15	0.30
k_sh	shaft dia. ratio = $\frac{OD_{shaft}}{OD_r}$	0.30	0.50
k_tp	rotor pole top ratio = $\frac{\tau_{r_top}}{\tau_r}$	0.40	0.80
k_rt	rotor pole root ratio = $\frac{\tau_{r_root}}{\tau_r}$	0.35	0.65
k_rr	rotor pole depth ratio = $\frac{\ell_{rpd}}{OD_r - ID_r}$	0.20	0.40

teeth, rotor teeth, and airgap were assigned denser meshes. A central composite design (CCD) method was employed to generate the requisite number of FEA parametric models, which were assessed and fitted using a regression curve to establish a relationship between independent variables and performance metrics [2]. The relationship was expressed through a polynomial function of the form:

TABLE 4. Independent variables for the OR-PM design optimization, and their ranges.

Variable	Description	Min	Max
k_sp	split ratio = $\frac{ID_r}{OD_r}$	0.75	0.80
k_pm	PM length ratio = $\frac{2 \cdot \ell_{PM}}{OD_s - ID_s}$	1.00	1.10
k_pm_l	PM width ratio = $\frac{\omega_{PM}}{g}$	2.00	8.00
k_br	bridge length ratio = $\frac{2 \cdot \ell_{bridge}}{OD_s - ID_s}$	0.40	0.50
k_h	slot length ratio = $\frac{2 \cdot \ell_{slot}}{OD_s - ID_s}$	0.40	0.50
k_l	slot width ratio = $\frac{\omega_{slot}}{\tau_s}$	0.40	0.50
k_tp	rotor pole top ratio = $\frac{\tau_{r_top}}{\tau_r}$	0.30	0.50
k_rt	rotor pole root ratio = $\frac{\tau_r}{\tau_r}$	0.40	0.70
k_rr	rotor pole depth ratio = $\frac{\ell_{rpd}}{OD_r - ID_r}$	0.40	0.50
k_sp_s	stator split ratio = $\frac{ID_s}{OD_s}$	0.40	0.50
k_st	stator extension ratio = $\frac{2 \cdot \ell_{se}}{OD_s - ID_s}$	0.25	0.30

$$Y = \beta_0 + \sum_{i=1}^{g_{\nu}} \beta_i X_{Ci} + \sum_{i=1}^{g_{\nu}} \beta_{ii} X_{Ci}^2 + \sum_{i=1}^{g_{\nu}} \sum_{j=i+1}^{d_{\nu}} \beta_{ij} X_{Ci} X_{Cj}.$$
 (5)

In this formulation, Y represents the response or performance parameter, β denotes the regression coefficients, and g_{ν} corresponds to the number of geometrical variables. The normalized value of the i^{th} factor is given by X_{Ci} , while x_i represents the actual i^{th} input factor. β_0 corresponds to the response parameter in this reference configuration, while coefficients β_{ii} and β_{ij} capture second-order effects. A large number of simulated designs were then extrapolated and analyzed using the response surface methodology (RSM) and box plots, with similar trends as those documented in [26]. This was done to study the influence of the geometrical variables on the performance metrics, visualize the trends, and determine optimal ranges for the geometric variables as summarized in Tables 1 - 4.

In line with expectations from the results summarized in Figs. 7 and 8, variables relating to the PM size and coil area impact the torque significantly, while the split ratios affect the motor losses, especially in the DC-excited topologies. The rotor geometry is closely tied to the torque ripple in all topologies, and the power factor has a distributed contribution from multiple variables in the different motor topologies. Due to non-linearities in the simulated responses of the proposed motor topologies, it has been found that all variables play a significant role in their various operations, and as such would be considered in a multi-objective optimization for best performance and mechanical stability of resultant designs.

B. PROBLEM FORMULATION AND OPTIMIZATION

Maximizing the torque output of a certain motor volume while achieving the highest possible efficiency is a typical goal for most manufacturers [44], [45]. Therefore, the parametric designs of the four motor topologies in inner and outer rotor configurations as shown in Figs. 5 and 6 were configured for outermost diameters of 10". The aim is to optimize all designs for an objective electromagnetic torque of 350Nm within the shortest stack length possible at a speed of 3,000rpm, resulting in a power of 100kW typical for industrial applications [46], [47].

Multi-objective optimization employing differential evolution (DE) and FEA was carried out to *minimize* two concurrent objectives relating to the ratio of stack length to average torque, \mathcal{F}_1 , and motor loss, \mathcal{F}_2 :

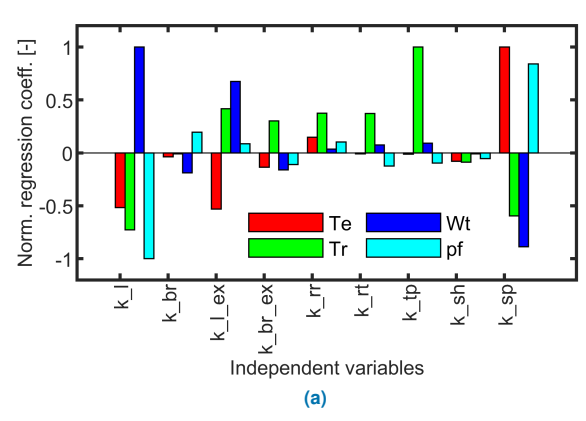
$$\mathcal{F}_1 = \frac{\ell_{stk}}{T_{avg}},$$

$$\mathcal{F}_2 = P_{loss} = P_{Cu} + P_{Fe},$$
(6)

where ℓ_{stk} is the stack length and T_{avg} is the average value of electromagnetic torque. The objective function for motor loss, P_{loss} , was calculated as the sum of the variable and constant losses of the motor, where P_{Fe} represents the core loss (constant losses) and P_{Cu} represents the copper loss (variable losses) at a current density of 30A/mm² with anticipated liquid cooling [42], [43]. At this current density and selected low-rated speed, the copper losses are expected to be dominant. The maximum value of core loss is considered in FEA to account for typical stray losses. It is assumed that PMs would be properly segmented and several thin steel laminations would be used, thereby mitigating eddy losses. Therefore, the combined copper and core losses would provide a fairly accurate model for the large-scale comparative analysis presented. Also, considering an anticipated high operating temperature, considerations have been taken in the selection of the B-H operating curves of the PMs as well as the loss calculations. This ensures a reduced sensitivity and variation in PM remanence and temperature-dependent degradation that would be observed between FEA and experimentation.

The optimization process employed is captured in the flowchart shown in Fig. 10. It follows an extensively researched pattern using DE as described in greater detail in [2], [7], [26]. A two-stage study is conducted to guarantee that each design achieves the target torque of 350Nm at a speed of 3,000rpm. Initially, the torque for each design is determined through finite element analysis (FEA). Afterward, the stack length of each design is adjusted to meet the required torque before it is evaluated for optimization goals and additional performance metrics.

A hybrid stopping criterion is implemented to improve the efficiency of the optimization process. This criterion allows the optimization to halt when either a maximum number of generations is reached or when minimal improvement is detected in three key points on the Pareto front over a few consecutive generations. The ranges for the independent variables that control the motor geometry as shown in Figs. 5 and 6 were further confirmed to be optimal by checking the distribution of variables from the Pareto designs with an



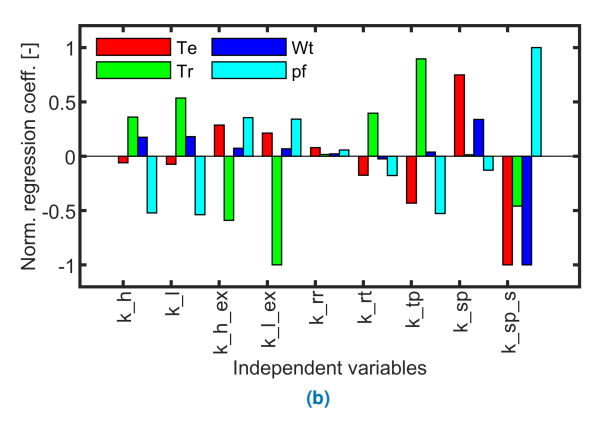
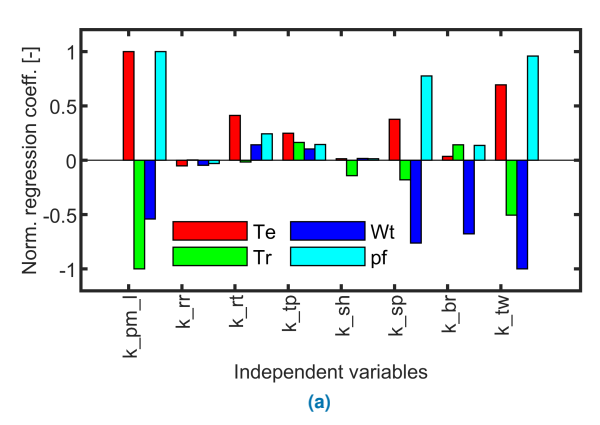


FIGURE 7. Normalized non-linear regression coefficients showing the influence of independent variables at peak loading on performance variables for (a) IR-DC, and (b) OR-DC.



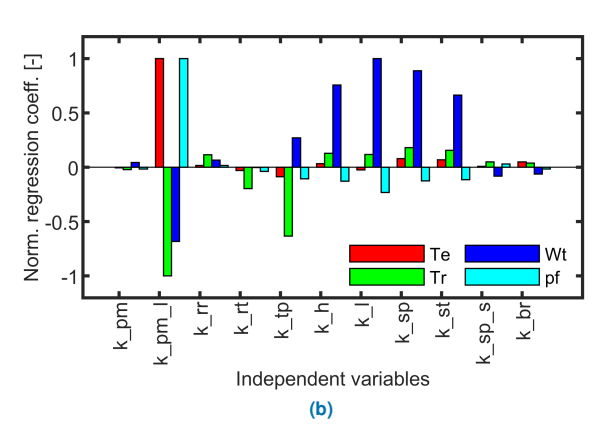


FIGURE 8. Normalized non-linear regression coefficients showing the influence of independent variables at peak loading on performance variables for (a) IR-PM, and (b) OR-PM.

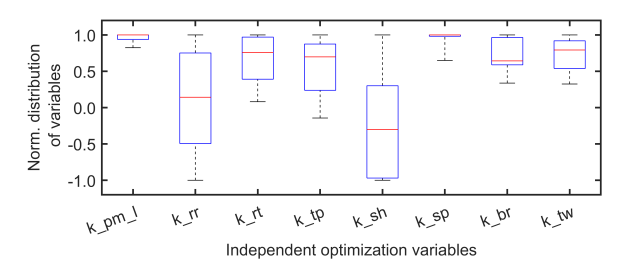


FIGURE 9. The distribution of variables for optimum Pareto front designs for the IR-PM configuration showing the uppermost limit is taken for variables relating to PM thickness, k_pm_l , and stator split, k_sp , in an attempt to maximize torque while reducing losses.

example box plot for the IR-PM shown in Fig. 9. The box plot reveals important characteristics of the Pareto-optimal solutions. Variables clustered around zero indicate optimal solutions tend toward the middle of their allowed ranges, while wide boxes or long whiskers suggest greater variability among optimal designs. The normalization enables direct comparison of all parameters on a common scale, -1.0 to +1.0 in the plot, despite their differing original ranges. In line with

expectations, for example, the thickness of PM, k_pm_l , and split ratio, k_sp , cling to the maximum limits to maximize torque while minimizing the motor losses, respectively.

C. RESULTS AND DISCUSSION

Following optimization of the inner and outer rotor topologies with PM and DC excitation in the previous section, the Pareto fronts and their projections are shown in Figs. 11 and 12. In line with expectations, PM-excited designs achieve the objective torque with the shortest stack lengths, particularly in IR-PM designs. DC-excited designs show higher losses, typically 2-3 times greater than PM-excited designs, since PMs are segmented with negligible losses while DC excitation windings produce additional copper losses. The outer rotor configurations generally have the benefit of a larger airgap which is beneficial for torque. This would result in reduced stack length for some designs with lower losses as compared to their inner rotor counterparts. The novel "wave" DC-excitation winding configuration in both inner (IR-WDC) and outer (OR-WDC) rotor configurations offers a performance compromise between PM and toroidal DC

TABLE 5. Performance comparison of selected "best" designs of the various motor topologies, all with a fixed torque constant, K_T , of 11.7Nm/A/mm².

Ref.	Torque	Torque ripple	Goodness	Active mass	Torque density	Specific torque
	[Nm]	[%]	$[\text{Nm}/\sqrt{W}]$	[kg]	[Nm/L]	[Nm/kg]
IR-DC	350	6	2.8	52	36.3	6.7
IR-WDC	350	7	3.3	34	49.3	10.2
IR-PM	350	9	4.5	25	65.2	14.0
OR-DC	350	15	3.1	44	31.2	8.0
OR-WDC	350	6	3.3	36	36.6	9.7
OR-PM	350	6	4.6	31	47.9	11.2

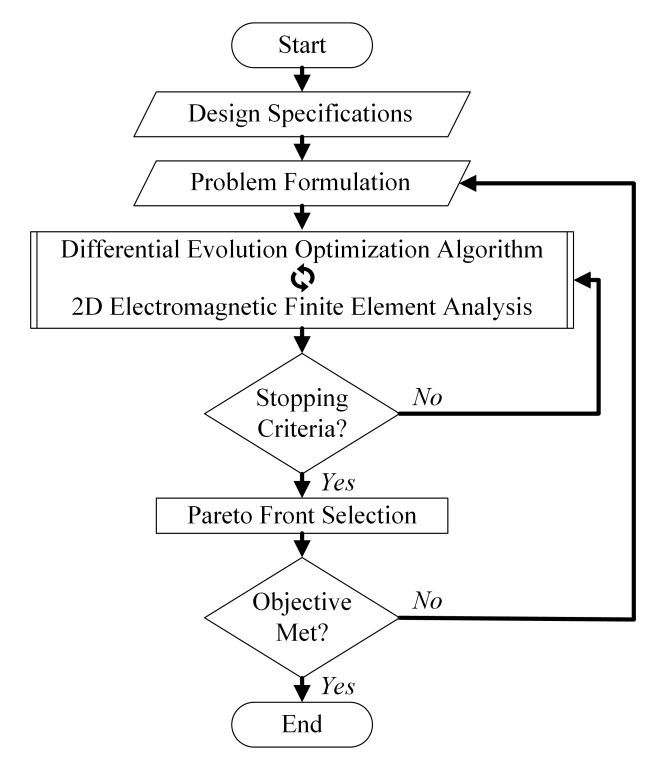


FIGURE 10. The implemented optimization algorithm is based on the differential evolution (DE) method. The Pareto designs would have the best compromise between the conflicting objectives.

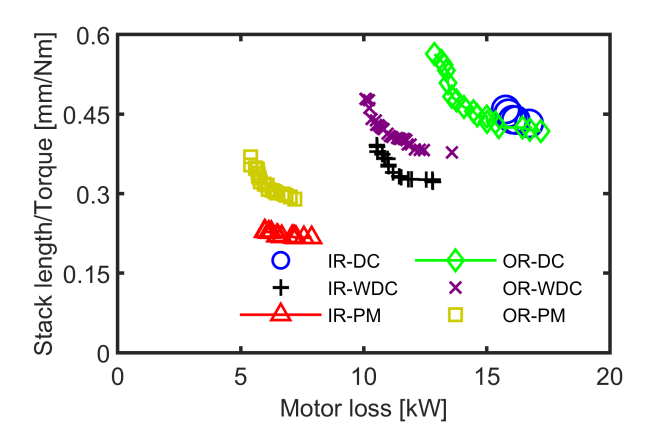


FIGURE 11. Optimization results: 2D Pareto front of objectives of stack length to average torque, and motor loss.

winding designs without demagnetization risk. Compared to toroidal implementation, the "wave" winding's shorter

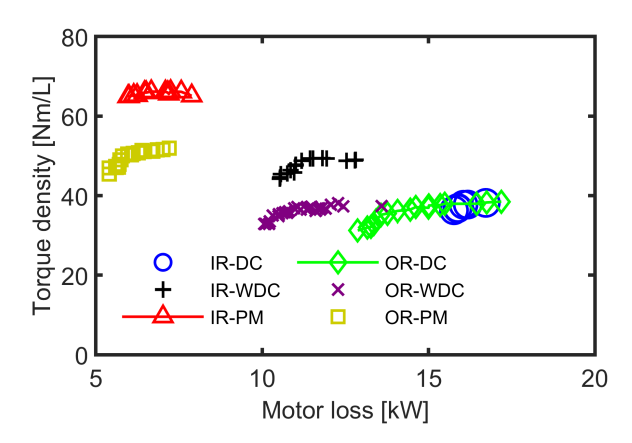


FIGURE 12. Optimization results: 2D Pareto front projection showing torque density.

TABLE 6. Performance comparison with high power density traction motors

	Type	Torque	Active mass	Torque-to- weight ratio
		[Nm]	[kg]	[Nm/kg]
IR-DC	New	350	52	6.7
IR-WDC	New	350	34	10.2
IR-PM	New	350	25	14.0
OR-DC	New	350	44	8.0
OR-WDC	New	350	36	9.7
OR-PM	New	350	31	11.2
Honda Accord 14	IPM (V)	306	33	9.3
YASA 400	Axial PM	360	24	15.0
Toyota Prius 10	IPM (V)	207	23	9.0
Chevrolet Bolt EV	IPM (V)	360	33	10.9
Tesla S	Induction	430	55	7.8

overall excitation winding length achieves reduced losses and higher goodness.

A projection of the Pareto designs in Fig. 12 shows the ranges of torque densities for the optimal designs, with the PM-excited designs being capable of about 25 - 50% higher torque density for the selected design specification. A performance comparison of the selected "best" designs from the obtained Pareto for the various topologies is shown in Tables 5 and 6. These designs have the highest machine goodness (which is the ratio of torque to the square root of losses) in their topology class and serve as example representatives. Typical values for machine goodness, active mass, torque density, and specific torque for the defined power rating are shown, as well as how they compare with documented per-

formance values for state-of-the-art electric motors [48]. Low torque ripple values, a critical performance metric for noise and vibration in these machine types, are achievable. These values can be further reduced through conventional skewing methods or advanced tooth shaping techniques as described in [41]. Also, the selected IR-PM design shows the most competitive performance in terms of active mass and torque-to-weight ratio, and may therefore be the most advantageous for prototyping, considering the ease of integration of an external stator configuration.

V. APPLICATION, PROTOTYPING, AND EXPERIMENTATION

A. OR-DC DESIGN FOR EV

Based on torque-loss analysis, an outer-rotor topology with toroidal DC excitation (OR-DC) may be an effective solution for typical light- and medium-duty EV applications. This configuration offers electromagnetic advantages, including a larger airgap and potentially higher power and torque density compared to inner-rotor implementations. Other benefits include, for example, the ease of manufacturing at a reduced cost, fault-tolerance, material availability, as well as zero demagnetization concerns. Toroidal coils in rectangular slots can benefit from established advanced windings such as the hairpin winding for high slot fill factor [49]-[51]. Also, considering the various degrees of freedom previously discussed for motor control, this motor can be operated for a wide torque-speed range given sufficient cooling. It is important to note that the final selection of a motor topology for any application would greatly depend on several factors including, for example, the ease of mechanical integration and cost.

The cross-sectional view of the selected "best" design for the OR-DC is shown in Fig. 13 with flux line and densities at a peak loading of 30A/mm² showing low saturation in the core. Its performance is summarized in Table 7 and its Ansys simulated efficiency map over an example speed range is shown in Fig. 14 [31]. The best performances can be seen in regions with high speeds around continuous torque. This performance indicates the motor may be well-suited for geared EV applications. Drive cycle analysis using k-means clustering has been performed for two example cases: the Orange County Transit Association and WLTP cycles. An example light EV was considered, with NREL drive cycle data analyzed to obtain the 7 most representative torquespeed points points (centroids). The corresponding energy weights (C.E.W) show the importance of each operating point, summing to 1, as shown in Tables 8 and 9. The first set of values can be used for a direct drive analysis while the second set shows the use of a gear ratio. Motor efficiency values were computed for these centroids using the reference 2D FEA design, as shown in Tables 8 and 9 respectively [33], [48]. Efficiency per cycle values of 90.0 and 95.2% were then obtained for the WLTP and Orange County drive cycles.

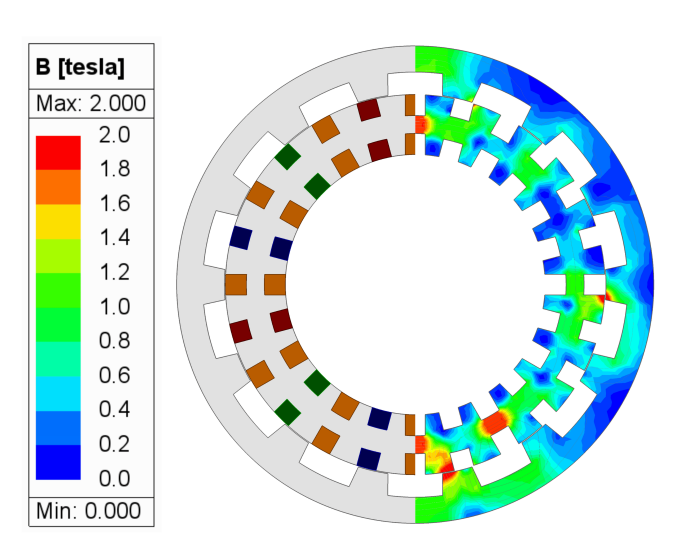


FIGURE 13. Cross-sectional view of selected "best" OR-DC design showing flux lines and densities at peak loading in one half.

TABLE 7. Performance summary of selected "best" OR-DC design

Parameter	Value	Unit
Peak torque	350	Nm
Continuous torque	73	Nm
Max. power	100	kW
Base speed	3,000	rpm
Emag eff. at peak torque	89.3	%
Emag eff. at continuous torque	91.0	%
Rotor OD	255	mm
Stack length	197	mm
Active mass	44	kg

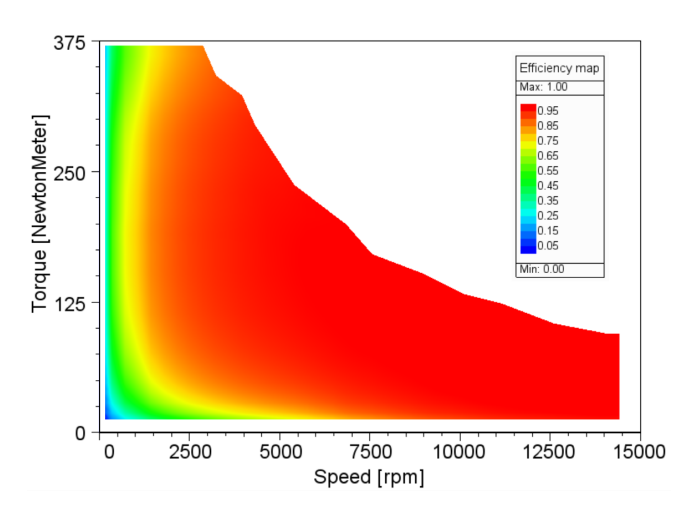


FIGURE 14. Simulated efficiency map of selected "best" OR-DC design showing its performance in constant torque and constant power regions; best performance occurs around the base speed and in the continuous torque regions.

B. IR-PM PROTOTYPE

Following the results of the comparative analysis, the IR-PM topology provides the best performance in terms of torque density and specific torque. Additional advantages for this topology in terms of manufacturing come from its traditional design with the rotor inner to the stator, which would reduce

TABLE 8. OR-DC Drive cycle analysis for the WLTP reporting the centroids and their corresponding energy weights (C.E.W).

Drive shaft			Motor shaft (assuming a gear ratio)			
Cent.	Torque	Speed	Torque	Speed	C.E.W	Motor eff.
no.	[Nm]	[rpm]	[Nm]	[rpm]	[-]	[%]
1	978	351	109	3157	0.263	90.6
2	1401	311	156	2796	0.232	90.0
3	553	325	61	2926	0.203	91.0
4	1920	187	213	1687	0.118	87.1
5	2462	163	274	1464	0.093	84.6
6	196	281	22	2529	0.063	90.4
7	2950	159	328	1434	0.029	83.0

TABLE 9. OR-DC Drive Cycle Analysis for Orange County Transit Association (31 minutes) reporting the centroids and their corresponding energy weights (C.E.W)

Drive shaft			Motor shaft (assuming a gear ratio)			
Cent.	Torque	Speed	Torque	Speed	C.E.W	Motor eff.
no.	[Nm]	[rpm]	[Nm]	[rpm]	[-]	[%]
1	1291	429	258	2146	0.208	88.3
2	946	560	189	2802	0.192	90.2
3	609	648	122	3240	0.190	90.4
4	351	743	70	3717	0.160	91.2
5	1783	442	357	2209	0.157	87.0
6	104	955	21	4775	0.090	91.0
7	87	88	17	442	0.001	73.5

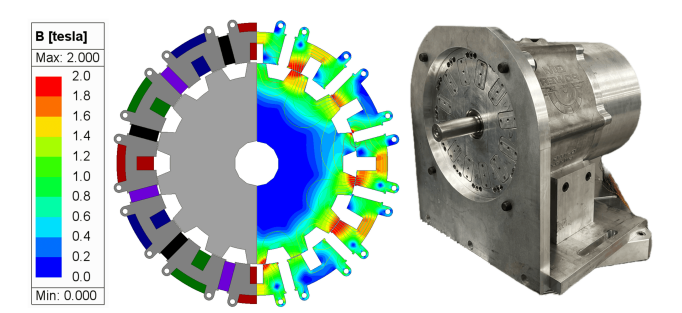


FIGURE 15. The 2-D FEA as-built model of the IR-PM design and the constructed prototype.

the complexity of integration. Also, with the external stator, established cooling techniques such as a cooling jacket can be applied for stator-only cooling.

The prototype for the IR-PM has been fabricated as shown in Fig. 15 with a rated power of 100kW at 3,000rpm, and a maximum tested power of 176kW with liquid cooling. The stator features 12 tangentially magnetized PMs and 12 stator segments for enhanced modularity. An M19-26G lamination material was used due to its lower cost and high availability, and the coils were hand-wound using a 23 AWG wire, achieving the designed slot fill factor of 0.5.

The test setup for the motor prototype is as shown in Fig. 16. A dynamometer (dyno) is coupled to the motor to apply mechanical loads, enabling performance testing across various torque and speed profiles. The motor is instrumented with 18 winding temperature sensors and one magnet temperature sensor to monitor thermal behavior, while a 6-wire resolver provides the rotor position and speed feedback. Additionally, 11 accelerometers are installed to measure vibrations, aiding

TABLE 10. Specifications and main dimensional properties of the 28-pole 3-phase IR-PM motor prototype.

Parameter	Value	Unit
Rated torque	319	Nm
Maximum speed	10,000	rpm
Airgap	0.5	mm
Stator OD	235	mm
Stack length	127	mm
Active mass	42	kg
No. of rotor protrusions	14	_

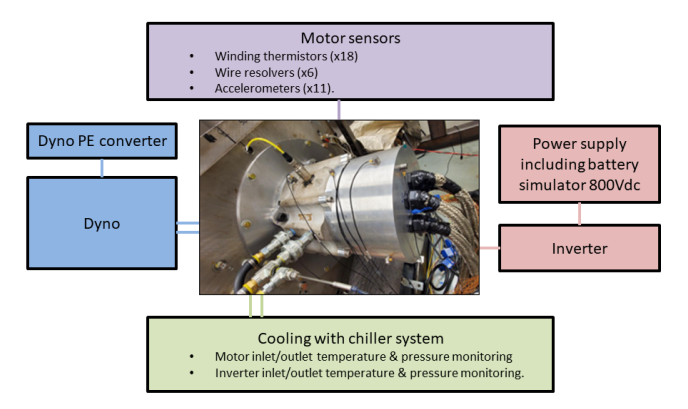


FIGURE 16. The test set-up for performance evaluation of the constructed IR-PM prototype.

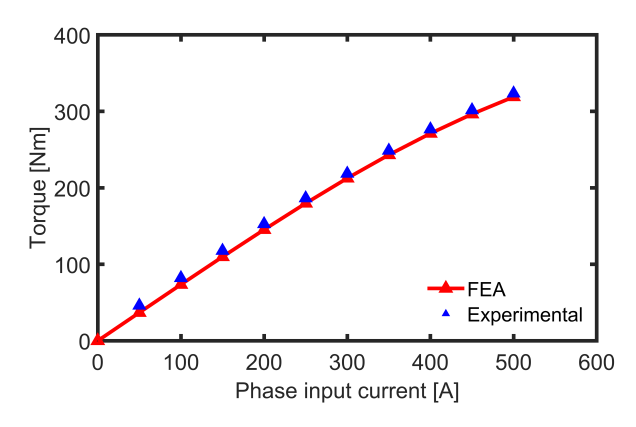


FIGURE 17. A comparison of the experimentally measured static torque with varying phase currents with results obtained from FEA for the PM prototype.

in the assessment of mechanical stability. The motor temperature is maintained via a cooling system, with pressure and temperature sensors to ensure effective thermal management.

Further evaluation involved comparing the results obtained from the 2D FEA analysis with those from experimental tests. The results of static torque measurements at various phase input currents are shown in Fig. 17, with satisfactory agreement between FEA and experimental results. Additionally, the prototype was tested at various torque-speed points to develop the efficiency map shown in Fig. 18, using measured values obtained at the high operating temperature of around 100°C. The rotor, which contains no active components, maintained a temperature reading that averaged between 25 - 35°C below the stator temperature.

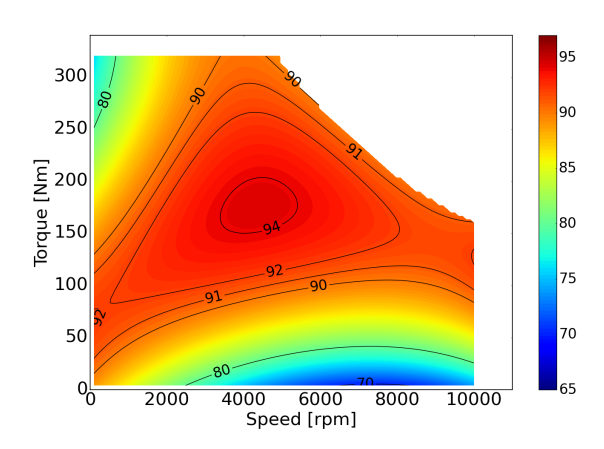


FIGURE 18. Measured efficiency map of the prototype machine at high operating temperature showing capability for high-efficiency operation.

Overall, a satisfactory correlation is obtained between 2D FEA and experimental results for this machine, confirming that the FEA model accurately represents the prototype under investigation. The high-efficiency values obtained at a high operating temperature also show its suitability for typical industrial applications.

VI. CONCLUSION

Synchronous motor topologies with PM or DC-excitation in an active stator are presented. These machines employ a simple reluctance rotor design with no active components, providing several advantages in manufacturing and high-efficiency operation. These machines can employ tangentially magnetized PMs for flux intensification or DC-excitation coils in the stator, which provides a PM-free operation, eliminating the typical risks associated with PMs. The stator can be manufactured in modules with slots adapted for high slot fill factors using the latest winding technology. The simple rotor enables high-speed operation and an extended range, with the potential for advanced stator-only cooling.

Through combined analytical and phenomenological analyses, it is shown that these synchronous machines operate through the interaction of the stator fields and the rotor, with the number of rotor protrusions determining the principal polarity of the machine. The control of the armature field, current phase angle, and excitation flux is also shown as the various degrees of freedom available in these motor topologies, making them highly advantageous. A novel design utilizing a "wave" DC-excitation winding was introduced, with the potential for reduced losses through shortened coil lengths compared to toroidal winding implementations in these PM-free designs.

A study of the geometry of motor topologies and their performance shows a highly non-linear relationship, and as such, established optimization methods such as those employing differential evolution should be used to obtain optimal designs. The selected "best" designs for each topology showed competitive performance against state-of-the-art electric motors. The inner rotor PM designs showed the most promise in torque density and specific torque.

The outer rotor design employing DC-excitation achieved an efficiency per cycle value of 95% for the selected drive cycle, indicating its promising suitability for EV application. A prototype of a selected inner rotor PM design was also experimentally tested, and the results showed a good correlation with those obtained from FEA, thereby offering validation. High values of efficiency were also obtained from the prototype at high operating temperatures.

ACKNOWLEDGMENT

Special thanks are due to Professor J.F. Eastham of University of Bath and Royal Academy of Engineering for the detailed review of this paper and for technical feedback. The support provided by QM Power Inc. for the experimental development, Ansys Inc. and University of Kentucky the L. Stanley Pigman Chair in Power endowment for computer software and hardware is gratefully acknowledged.

REFERENCES

- W. Li, H. Ding, N. Xu, and J. Zhang, "Toward carbon-neutral transportation electrification: A comprehensive and systematic review of eco-driving for electric vehicles," IEEE Transactions on Transportation Electrification, vol. 10, no. 3, pp. 6340–6360, 2024.
- [2] M. Rosu, P. Zhou, D. Lin, D. M. Ionel, M. Popescu, F. Blaabjerg, V. Rallabandi, and D. Staton, Multiphysics simulation by design for electrical machines, power electronics and drives. John Wiley & Sons, 2017.
- [3] B. Sarlioglu, Y. Zhao, and T. Lipo, "A novel doubly salient single phase permanent magnet generator," in Proceedings of 1994 IEEE Industry Applications Society Annual Meeting, vol. 1, 1994, pp. 9–15 vol.1.
- [4] Y. Amara, H. B. Ahmed, and M. Gabsi, Hybrid Excited Synchronous Machines: Topologies, Design and Analysis. John Wiley & Sons, 2023, ISBN: 9781786306852.
- [5] X. Zhu, C. H. T. Lee, C. C. Chan, L. Xu, and W. Zhao, "Overview of flux-modulation machines based on flux-modulation principle: Topology, theory, and development prospects," IEEE Transactions on Transportation Electrification, vol. 6, no. 2, pp. 612–624, 2020.
- [6] C. Contò and N. Bianchi, "A hybrid-excitation synchronous motor with a change in polarity," Machines, vol. 10, no. 10, 2022. [Online]. Available: https://www.mdpi.com/2075-1702/10/10/869
- [7] O. A. Badewa, A. Mohammadi, D. D. Lewis, S. Essakiappan, M. Manjrekar, and D. M. Ionel, "Electromagnetic design characterization of synchronous machines with flux switching effect employing reluctance rotors and stators with pms and ac concentrated coils," IEEE Transactions on Industry Applications, vol. 61, no. 3, pp. 3796–3808, 2025.
- [8] L. Carr, "Induction-type synchronous motors," Journal of the Institution of Electrical Engineers, vol. 60, no. 306, pp. 165–174, 1922.
- [9] A. K. Das Gupta, An analysis of one type of inductor alternator. University of Wisconsin-Madison, 1958.
- [10] S. E. Rauch and L. J. Johnson, "Design principles of flux-switch alternators [includes discussion]," Transactions of the American Institute of Electrical Engineers. Part III: Power Apparatus and Systems, vol. 74, no. 3, pp. 1261–1268, 1955.
- [11] Y. Liao, F. Liang, and T. Lipo, "A novel permanent magnet motor with doubly salient structure," IEEE Transactions on Industry Applications, vol. 31, no. 5, pp. 1069–1078, 1995.
- [12] R. Deodhar, S. Andersson, I. Boldea, and T. Miller, "The flux-reversal machine: a new brushless doubly-salient permanent-magnet machine," IEEE Transactions on Industry Applications, vol. 33, no. 4, pp. 925–934, 1997
- [13] L. Parsa and H. A. Toliyat, "Fault-tolerant interior-permanent-magnet machines for hybrid electric vehicle applications," IEEE Transactions on Vehicular Technology, vol. 56, no. 4, pp. 1546–1552, 2007.

- [14] I. Boldea, L. N. Tutelea, L. Parsa, and D. Dorrell, "Automotive electric propulsion systems with reduced or no permanent magnets: An overview," IEEE Transactions on Industrial Electronics, vol. 61, no. 10, pp. 5696– 5711, 2014.
- [15] A. Takbash, M. Ibrahim, and P. Pillay, "Design optimization of a spoketype variable flux motor using AlNiCo for electrified transportation," IEEE Transactions on Transportation Electrification, vol. 4, no. 2, pp. 536–547, 2018
- [16] H. Chen, A. M. EL-Refaie, and N. A. O. Demerdash, "Flux-switching permanent magnet machines: A review of opportunities and challenges—part I: Fundamentals and topologies," IEEE Transactions on Energy Conversion, vol. 35, no. 2, pp. 684–698, 2020.
- [17] O. A. Badewa and D. M. Ionel, "Analysis and design of synchronous machines with reluctance rotor and PM stator combined excitation," in 2024 IEEE Energy Conversion Congress and Exposition (ECCE), 2024.
- [18] I. Boldea, L. N. Tutelea, and A. A. Popa, "Reluctance synchronous and flux-modulation machines designs: Recent progress," IEEE Journal of Emerging and Selected Topics in Power Electronics, vol. 10, no. 2, pp. 1683–1702, 2022.
- [19] C. S. Goli, M. G. Kesgin, P. Han, D. M. Ionel, S. Essakiappan, J. Gafford, and M. D. Manjrekar, "Analysis and design of an electric machine employing a special stator with phase winding modules and pms and a reluctance rotor," IEEE Access, vol. 12, pp. 9621–9631, 2024.
- [20] J. Faiz and M. Maktobian, "Performance enhancement of flux switching motor for electric vehicle applications: an overview," IET Electrical Systems in Transportation, vol. 2024, no. 1, p. 9071667, 2024.
- [21] H. C. Idoko, U. B. Akuru, O. Popoola, W. Ullah, F. Khan, and L. Masisi, "Parametric evaluation and electromagnetic performance comparison of conventional and double-stator wound-field flux switching machines," IEEE Transactions on Industry Applications, pp. 1–11, 2025.
- [22] K. P. Schneider, S. Simizu, M. E. McHenry, and M. P. de Boer, "Optimization study of rare earth-free metal amorphous nanocomposite axial flux-switching permanent magnet motor," Energies, vol. 18, no. 3, p. 640, 2025.
- [23] O. A. Badewa, A. Mohammadi, D. D. Lewis, and D. M. Ionel, "Optimal design and comparison of synchronous machines with inner and outer reluctance rotors and pm or dc stator combined excitation," in 2024 IEEE Energy Conversion Congress and Exposition (ECCE), 2024, pp. 5461– 5465.
- [24] B. Ullah, F. Khan, Z. Ahmad, S. Akbar, A. H. Milyani, and A. A. Azhari, "Performance analysis of a modular e-shaped stator hybrid excited flux switching motor with flux gaps," IEEE Access, vol. 10, pp. 116 098– 116 106, 2022.
- [25] H. Ali, E. Sulaiman, R. Aziz, M. Jenal, M. Z. Ahmad, and F. Khan, "Review of double stator flux switching machines with various arrangements of excitation sources," Alexandria Engineering Journal, vol. 60, no. 5, pp. 4393–4410, 2021.
- [26] A. Mohammadi, O. A. Badewa, Y. Chulaee, D. D. Lewis, S. Essakiappan, M. Manjrekar, and D. M. Ionel, "Design optimization of a direct-drive wind generator with a reluctance rotor and a flux intensifying stator using different PM types," IEEE Transactions on Industry Applications, pp. 1– 10, 2024.
- [27] O. A. Badewa, A. Mohammadi, D. D. Lewis, D. M. Ionel, S. Essakiappan, and M. Manjrekar, "Optimization of an electric vehicle traction motor with a PM flux intensifying stator and a reluctance outer rotor," in 2023 IEEE Transportation Electrification Conference & Expo (ITEC), 2023.
- [28] O. A. Badewa, A. Mohammadi, D. M. Ionel, S. Essakiappan, and M. Manjrekar, "Electric vehicle traction motor with a reluctance outer rotor and a modular stator with AC concentrated toroidal windings and PM or DC wave winding excitation," in 2023 IEEE Energy Conversion Congress and Exposition (ECCE), 2023, pp. 3845–3850.
- [29] D. D. Lewis, D. R. Stewart, M. Vatani, O. A. Badewa, A. Mohammadi, and D. M. Ionel, "Fault-tolerant topologies with halbach array and pm-free multi-stage multi-module electric machines for electric aircraft propulsion," in 2024 IEEE Energy Conversion Congress and Exposition (ECCE), 2024, pp. 2524–2528.
- [30] D. D. Lewis, O. A. Badewa, A. Mohammadi, M. Vatani, and D. M. Ionel, "Fault tolerant electric machine concept for aircraft propulsion with pm rotor and dc current stator dual-stage excitation," in 2023 12th International Conference on Renewable Energy Research and Applications (ICRERA), 2023, pp. 607–611.
- [31] Ansys® Electronics, Maxwell, version 24.1, 2024, ANSYS Inc.
- [32] E. Sayed, S. M. Castano, J. W. Jiang, J. Liang, G. Pietrini, M. H. Bakr, A. Emadi, and B. Bilgin, "Design of multilayer concentric ferrite-magnet

- machines for a traction application," IEEE Transactions on Transportation Electrification, vol. 7, no. 3, pp. 1548–1560, 2021.
- [33] O. A. Badewa and D. M. Ionel, "Comparative analysis of motors with inner and outer reluctance rotors and PM stators," in 2024 IEEE Transportation Electrification Conference and Expo (ITEC), 2024, pp. 1–6.
- [34] N. Taran, D. M. Ionel, V. Rallabandi, G. Heins, and D. Patterson, "An overview of methods and a new three-dimensional FEA and analytical hybrid technique for calculating AC winding losses in PM machines," IEEE Transactions on Industry Applications, vol. 57, no. 1, pp. 352–362, 2021.
- [35] A. Fatemi, D. M. Ionel, N. A. O. Demerdash, D. A. Staton, R. Wrobel, and Y. C. Chong, "Computationally efficient strand eddy current loss calculation in electric machines," IEEE Transactions on Industry Applications, vol. 55, no. 4, pp. 3479–3489, 2019.
- [36] S. Lee, W. Lee, M. Liu, and B. Sarlioglu, "High-frequency motor impedance analysis and CM current estimation of electric motors with concentrated and toroidal windings," IEEE Transactions on Transportation Electrification, pp. 1–1, 2024.
- [37] M. Popescu and D. G. Dorrell, "Proximity losses in the windings of high speed brushless permanent magnet AC motors with single tooth windings and parallel paths," IEEE Transactions on Magnetics, vol. 49, no. 7, pp. 3913–3916, 2013.
- [38] A. Mohammadi, O. A. Badewa, Y. Chulaee, and D. M. Ionel, "Two-level design optimization of ac machines with dc stator excitation and minimal torque ripple using reluctance rotor profile shaping," in 2024 IEEE Energy Conversion Congress and Exposition (ECCE), 2024, pp. 5174–5179.
- [39] J. Ma, L. Wu, and Z. Q. Zhu, "Effect of magnet thickness on electromagnetic performance of high speed permanent magnet machines," in 2017 IEEE International Electric Machines and Drives Conference (IEMDC), 2017, pp. 1–7.
- [40] M. Popescu, L. Di Leonardo, G. Fabri, G. Volpe, N. Riviere, and M. Villani, "Design of induction motors with flat wires and copper rotor for e-vehicles traction system," IEEE Transactions on Industry Applications, vol. 59, no. 3, pp. 3889–3900, 2023.
- [41] A. Mohammadi, O. A. Badewa, Y. Chulaee, and D. M. Ionel, "Two-level multi-objective design optimization including torque ripple minimization for stator excited synchronous and flux switching machines," IEEE Access, vol. 13, pp. 80 857–80 870, 2025.
- [42] A. Fatemi, D. M. Ionel, N. A. O. Demerdash, and T. W. Nehl, "Optimal design of ipm motors with different cooling systems and winding configurations," IEEE Transactions on Industry Applications, vol. 52, no. 4, pp. 3041–3049, 2016.
- [43] R. Wang, X. Fan, D. Li, R. Qu, L. Li, and T. Zou, "Convective heat transfer characteristics on end-winding of stator immersed oil-cooled electrical machines for aerospace applications," IEEE Transactions on Transportation Electrification, vol. 8, no. 4, pp. 4265–4278, 2022.
- [44] A. Mohammadi, Y. Chulaee, A. M. Cramer, I. G. Boldea, and D. M. Ionel, "Large-scale design optimization of an axial-flux vernier machine with dual stator and spoke PM rotor for EV in-wheel traction," IEEE Transactions on Transportation Electrification, pp. 1–1, 2024.
- [45] L. Shao, R. Navaratne, M. Popescu, and G. Liu, "Design and construction of axial-flux permanent magnet motors for electric propulsion applications—a review," IEEE Access, vol. 9, pp. 158 998–159 017, 2021.
- [46] G. Cakal and B. Sarlioglu, "Two-phase immersion cooling of highperformance electric traction motors," IEEE Transactions on Transportation Electrification, pp. 1–1, 2024.
- [47] B. Fahimi, L. H. Lewis, J. M. Miller, S. D. Pekarek, I. Boldea, B. Ozpineci, K. Hameyer, S. E. Schulz, A. Ghaderi, M. Popescu, B. Lehman, and D. D. Patel, "Automotive electric propulsion systems: A technology outlook," IEEE Transactions on Transportation Electrification, vol. 10, no. 3, pp. 5190–5214, 2024.
- [48] A. Fatemi, D. M. Ionel, M. Popescu, Y. C. Chong, and N. A. O. Demerdash, "Design optimization of a high torque density spoke-type PM motor for a formula E race drive cycle," IEEE Transactions on Industry Applications, vol. 54, no. 5, pp. 4343–4354, 2018.
- [49] K. Kalengo, M. Bharathi, U. B. Akuru, and O. M. Popoola, "Sizing and comparative performance evaluation of a 5 kW DC-excited flux reversal direct-drive wind generator," in 2024 32nd Southern African Universities Power Engineering Conference (SAUPEC), 2024, pp. 1–6.
- [50] N. Tang, D. Sossong, N. Krause, X. Hou, M. J. Liben, D. C. Ludois, and I. P. Brown, "Implementation of a metamodel-based optimization for the design of a high power density wound field traction motor," IEEE Transactions on Industry Applications, vol. 59, no. 6, pp. 6726–6735, 2023.

[51] W. Zhang, Z. Wu, Y. Fan, W. Hua, and M. Cheng, "Analysis and improvement of DC winding current dynamics in wound field switched flux machine," IEEE Transactions on Industry Applications, vol. 60, no. 4, pp. 6023–6032, 2024.



OLUWASEUN A. BADEWA (Graduate Student Member, IEEE) received the B.Sc. degree from ATBU, Bauchi, Nigeria, and the M.Sc. degree from CAU, Kiel, Germany both in Electrical engineering. From 2016 to 2020, he worked as a Senior Electrical engineer with DORCL, Nigeria specialized in electrical design and detailed engineering, and commissioning for petrochemical complexes. He is currently working toward the Ph.D. degree with SPARK Laboratory, Department of Electri-

cal and Computer Engineering, University of Kentucky, Lexington, KY, USA. He was the co-recipient of the Best Paper Award at the 2022 IEEE International Conference on Renewable Energy Research and Applications (ICRERA) with a paper on multi-MW direct-drive wind-turbine generators employing a flux-intensifying PM stator and reluctance rotor novel topology. At UK, he has been working as a Research Assistant with research interests in electric machines and power electronic drives.



ALI MOHAMMADI (Senior Member, IEEE) received his B.Sc. and M.Sc. degrees in electrical engineering from Babol Noshirvani University of Technology, Iran, in 2016 and 2020, respectively, and his Ph.D. from the University of Kentucky, USA, in 2025. His research focuses on electric machine design and optimization, motor drives, power electronics, transportation electrification, and renewable energy systems. He has contributed to NSF-, NASA-, and industry-sponsored projects

and received multiple honors, including the IEEE Transactions on Energy Conversion Best Paper Award. Dr. Mohammadi was recognized with Best Paper Awards at the 2022 IEEE International Conference on Renewable Energy Research and Applications (ICRERA), the 2023 IEEE Transportation Electrification Conference (ITEC), and the 2023 IEEE ICRERA. He also received Best Student Demonstration Awards at the 2024 IEEE Energy Conversion Congress and Exposition (ECCE) and the 2025 IEEE International Electric Machines and Drives Conference (IEMDC).



SOMASUNDARAM ESSAKIAPPAN (Senior Member, IEEE) received the B.E. degree in Electrical and Electronics Engineering from the College of Engineering Guindy, in 2007, and the M.S. and Ph.D. degrees in Electrical Engineering from Texas A&M University, in 2010 and 2014, respectively. He has been a Lead Electrical Engineer for Advanced Technologies at Trane Technologies since 2024, and an Adjunct Professor with the Department of Electrical and Computer Engineer-

ing, The University of North Carolina at Charlotte, since 2015. Previously, he was an R&D Engineering Manager with QM Power Inc., responsible for leading programs on new motor architectures and motor drives, from 2021 to 2023. Prior to that, he was a Teaching Professor and the Manager of the Flexible Energy Laboratories, Energy Production and Infrastructure Center, The University of North Carolina at Charlotte, from 2016 to 2021, where he developed and managed a high-power research and industrial testing laboratory for power electronic systems. He has published more than 50 research articles in various disciplines of power engineering and is an inventor of two U.S. patents and multiple pending patent applications. His research interests include power electronics for distributed energy integration, power quality and resiliency, and motors and drives. He is an active volunteer in professional societies and serves as a member of the Power Electronics Society Magazine Advisory Board and a reviewer for major journals and conferences. In the past, he has served as the Chair of the Young Professionals of IEEE Power Electronics Society, the Technical Program Chair for the 9th and 12th editions of the International Symposium on Power Electronics for Distributed Generation Systems (IEEE-PEDG), and the Publications Chair for the 10th and 11th Workshops on Wide Bandgap Power Devices and Applications (IEEE-WiPDA).



DONOVIN D. LEWIS (Member, IEEE) received the B.Sc. degree in electrical engineering in 2021 from the University of Kentucky, Lexington, KY, USA, where he is working toward the Ph.D. degree with the SPARK Laboratory, Department of Electrical and Computer Engineering. He is also a remote research collaborator with Oak Ridge National Laboratory, and a summer visitor with the University of Oxford, Oxford, England. During his undergraduate studies, he was a William C. Parker

Scholar, a NASA REU student, a recipient of the IEEE PES Plus Scholarship, and the Chief Electrical Engineer of the 2021 U.S. National Champion University of Kentucky Solar Car Team. He is currently a National Science Foundation (NSF) Graduate Research Fellow, was a University of Kentucky Otis A. Singletary Graduate Fellow, and has been recognized by the UK Stanley and Karen Pigman COE with the 2024 Outstanding PhD Student Award. His research interests include wireless charging of electric vehicles, electric motors, and renewable energy integration.



MADHAV D. MANJREKAR (Senior Member, IEEE) was born in 1972. He received the B.E. degree from the Government College of Engineering, University of Pune, India, in 1993, the M.Tech. degree from the Center for Electronic Design and Technology, Indian Institute of Science, India, in 1995, the M.S. degree from Montana State University, Bozeman, in 1997, the Ph.D. degree in electrical engineering from the University of Wisconsin, Madison, in 1999, and joined the

University of North Carolina – Charlotte as an Associate Professor of Electrical & Computer Engineering in 2012. Prior to joining academia, he worked as the Vice President of Global Research and Innovation at Vestas, and previously has held various leadership and management positions at Siemens, Eaton and ABB. Dr. Manjrekar holds over 10 US and international patents, has published over 125 journal and conference papers, and has received multiple IEEE prize paper awards. He has advised over 30 PhD and MS students and currently serves as an Assistant Director and Chief Research Officer of the Energy Production and Infrastructure Clauder (EPDES) at the university.



DAN M. IONEL (Fellow, IEEE) received both the M.Eng. and Ph.D. degrees in electrical engineering from the Polytechnic University of Bucharest, Bucharest, Romania. His doctoral studies included a Leverhulme Visiting Fellowship with the University of Bath, Bath, U.K. He was a Postdoctoral Researcher with the SPEED Laboratory, University of Glasgow, Glasgow, U.K.

Previously to 2015, he worked in industry, most recently as Chief Engineer with Regal Beloit

Corp., Grafton, WI, USA, and before that as Chief Scientist with Vestas Wind Turbines. He was also a Visiting Professor and a Research Professor with the University of Wisconsin and Marquette University, Milwaukee, WI, USA. He is currently Professor and the L. Stanley Pigman Chair in Power with the University of Kentucky, Lexington, KY, USA, where he is also the Director of the Power and Energy Institute of Kentucky and of the SPARK Laboratory. During his 2024 sabbatical in England, U.K., he was a Leverhulme Visiting Professor with University of Bath, expanding also the collaboration with University of Oxford, and was appointed as an Honorary Professor at University College London (UCL).

Dr. Ionel has contributed to technological developments with long-lasting industrial impact, designed electric machines and drives with ratings between 0.002 and 10,000hp. He holds more than 40 patents, and has authored or coauthored two books and more than 300 technical papers, including IEEE award winners. He served as chair of large committees and conferences for the IEEE power societies, and editor of journals. Dr. Ionel received the Cyril G. Veinott Award, the highest distinction for electromechanical energy conversion contributions from the IEEE PES.